

Effect of polarization force on the Mach cones in a complex plasma

P. Bandyopadhyay^{1,2}, K. Jiang^{1,3}, R. Dey⁴, G. E. Morfill¹¹

¹ Max-Planck Institut für Extraterrestrische Physik, D-85741, Garching, Germany

² Institute for Plasma Research, Bhat, Gandhinagar-382428, India

³ Infineon Technologies AG, Am Campeon 1-12, D-85579 Neubiberg, Germany

⁴ Max-Planck Institut für Plasma Physik, Boltzmannstr. 2, 85748, Garching, Germany

We report the modifications of compressional Mach cone propagation characteristics due to the polarization force acting on micron size dust particles embedded in a non-uniform plasma. We solve the hydrodynamic fluid equations for highly charged dust particles to investigate the Mach cone by incorporating the polarization force in the momentum equation and observe the structural change on lateral wakes at different polarization force for a given Mach number and Epstein drag force. We also notice that the maximum amplitude of normalized dust density perturbation decreases with the increase of polarization interaction when the other parameters remain constant.

I. INTRODUCTION

Mach cones are V-shaped disturbances or shock waves produced by a supersonic/subsonic object moving through a medium. Cone-shaped pattern left behind the trails of a duck or boat/ship in water motivates the researchers to explore it in their respective fields. Complex plasma (or dusty plasma)¹⁻⁴, which consists of electrons, ions and micron sized charge dust grains, serves as an excellent medium in which wake structures can be easily excited. Over the past decade, there has been a great deal of interest in understanding the Mach cone structures excited by a moving disturbance in a complex plasma both theoretically⁵⁻¹⁴ and experimentally¹⁵⁻²¹. The existence of Mach cone in complex plasma was first predicted by Havnes *et al.*^{5,6} and later it was experimentally observed by Samsonov *et al.*^{15,16} and Melzer *et al.*¹⁷ in a 2D plasma crystal. In the above experiments the compressional Mach cones were excited either by a charged particle moving spontaneously beneath the 2D lattice^{15,16} or by radiation pressure from a well focused laser beam scanning across a 2D crystal¹⁷. Later on, Nosenko *et al.*^{18,19} performed an experiment on shear driven Mach cone which was composed of a single cone. Motivated by these experimental observations on different kinds of wake structures, a number of theoretical models have been proposed to explain the experimental findings. Dubin⁷ claimed that the Mach cones are the superposition of linear dispersive waves excited by the moving disturbance which was verified by Ma and Bhattacharjee⁸ by performing Molecular Dynamic (MD) simulations for compressional Mach cones in the far field approximations.

An attention has also been paid to study the Mach cone under the micro-gravity ($\sim 0g$) conditions²² in a three dimensional crystal/fluid. Couple of experimental observations of 3D Mach cone were reported independently by Jiang *et al.*²⁰ and Mierk *et al.*²¹ under the $0g$ condition on board International Space Station. An observation of single cone Mach structure²⁰ was reported for the first time in a 3D fluid and the results were compared with a hydrodynamic model. Soon after, the speed of sound was measured directly by exciting a double Mach cone

structure using a supersonic particle of Mach number $M \lesssim 3$ ²¹. However, a theoretical description of shear-wave Mach cone in a 3D strongly coupled complex plasma has already been proposed by Bose *et al.*²³ by developing a generalized hydrodynamic model to describe the formation of single Mach cone structure.

Recently, a series of theoretical studies has been performed to investigate the propagation characteristics of linear and non-linear Dust Acoustic Waves (DAWs) in the presence of polarization force acting on dust grains in a background of non-uniform plasmas²⁴⁻²⁶. The concept of polarization force and its importance in dusty plasma physics were first discussed by Hamaguchi and Farouki^{27,28}. The polarization force arises due to any kind of deformation of the Debye sheath around the dust grains in the background of non-uniform plasmas. Non-uniformity in plasmas arises due to non-zero gradient of local electron and ion density and/or their temperatures. According to Hamaguchi and Farouki^{27,28}, the polarization force acting on the micron size dust particles can be expressed as, $F_p = -Q^2 \nabla \lambda_d / 8\pi \epsilon_0 \lambda_d^2$, where $Q = -Z_d e$ is the average charge (Z_d represents the charge number) on each particle and λ_d is the Debye radius of plasma which can be defined as $\lambda_d = \lambda_{de} \lambda_{di} / \sqrt{\lambda_{di}^2 + \lambda_{de}^2}$ with $\lambda_{di(e)}$ being the ion (electron) Debye radius and is given by $\lambda_{di(e)} = (\epsilon_0 k_B T_{i(e)} / n_{i(e)} e^2)^{1/2}$, $T_{i(e)}$ and $n_{i(e)}$ are the temperature and density of ions (electrons), respectively. The main features of polarization force are a) it always acts opposite to the electrostatic force, b) it is independent of polarity of dust grains, and c) it arises because of polarization of plasma ions around the negatively charged dust grains. The effect of polarization force was first applied by Khrapak *et al.*²⁴ to investigate the propagation characteristic of DAW. They showed that the wave phase velocity of DAWs decreases with the increase of the strength of polarization force. They also mentioned that the effect of polarization force on dust particles is pronounced for bigger particles. However, there exists a critical dust size beyond which the net force on the dust grains is no longer a restoring force and the dispersion relation admits a transition from propagating DAWs to periodically growing perturbations. The threshold limit on dust grain size depends on plasma parameters and

for a typical gas discharge plasma the threshold limit is $\sim 10 \mu\text{m}$. The earlier studies on Dust Acoustic Solitary Waves (DASWs)^{25,26} also showed considerable modifications of propagation characteristics in the presence of polarization force.

In this article, we investigate the propagation characteristics of Mach cone in the presence of polarization force acting on micron sized charged dust particles in a background of non-uniform plasma. We construct the expressions for the perturbed dust density and the velocity vector field by solving the hydrodynamic model for dust fluids assuming electrons and ions to be Boltzmannian. By performing a detailed study, we conclude that the polarization force plays an important role to determine the Mach cone structures. We also notice that the amplitude of perturbed density reduces with the increase of polarization force when the other parameters remain constant.

The paper is organized as follows. In the next section we discuss the model equations that include the effects of polarization force. In Section III, we discuss our numerical results. A brief concluding remark will be made in section IV.

II. THEORETICAL MODEL

In the standard fluid model of dusty plasma for studying low frequency phenomena in the regime where the dust dynamics are important, it is necessary to consider the electrons and ions as light fluids and can be described by Boltzmann distribution and to use the full set of hydrodynamic equations to describe the dust dynamics. The densities of electrons and ions at temperature T_e and T_i can be written as,

$$\begin{aligned} n_e &= n_{eo} \exp(e\phi(\mathbf{r}, t)/k_B T_e), \\ n_i &= n_{io} \exp(-e\phi(\mathbf{r}, t)/k_B T_i). \end{aligned} \quad (1)$$

Here, $n_{eo}(n_{io})$ is the equilibrium density of electrons (ions) and $\phi(\mathbf{r}, t)$ is the electrostatic potential in a Cartesian coordinate system with $\mathbf{r}(x, y, z = 0)$ of a 2D system. e and k_B denote the electronic charge and the Boltzmann constant, respectively.

The fluid equations *i.e.*, the continuity, the momentum and the Poisson equation for the dust component in our system can be written as, respectively,

$$\frac{\partial n_d(\mathbf{r}, t)}{\partial t} + \nabla \cdot [n_d(\mathbf{r}, t) \mathbf{v}_d(\mathbf{r}, t)] = 0, \quad (2)$$

$$m_d \frac{\partial \mathbf{v}_d(\mathbf{r}, t)}{\partial t} + m_d \mathbf{v}_d \nabla \cdot \mathbf{v}_d(\mathbf{r}, t) = Z_d e \nabla \phi(\mathbf{r}, t) + \mathbf{F}_{EP} + \mathbf{F}_p, \text{ and} \quad (3)$$

$$\nabla^2 \phi(\mathbf{r}, t) = \frac{e}{\epsilon_0} [Z_d n_d(\mathbf{r}, t) + Z_t \delta(\mathbf{r} - \mathbf{u}t) + n_e(\mathbf{r}, t) - n_i(\mathbf{r}, t)]. \quad (4)$$

In the above equations, $n_d(\mathbf{r}, t)$ and $\mathbf{v}_d(\mathbf{r}, t)$ represent the instantaneous number density and the velocity vector of

the dust fluid, respectively. m_d denotes the mass of dust particles. In our calculations systematic or stochastic dust charge variations are neglected.

We also include a δ -function in the Poisson equation (Eq. 4) to incorporate the presence of projectile particle which moves with velocity \mathbf{u} and charge number Z_t . The projectile particle in our paper is represented as a point charge and this is only applicable when the particle size is relatively small comparing to the scale of the Mach cone phenomena. Studies with particular interests in finite sized projectiles or evidently bigger than those forming the complex plasma medium are out of the scope of this paper, but could be conducted by means of PIC simulations^{29,30}. Generally as it is well known that in gas dynamics, the supersonic object creates a U-shaped Mach cone when it is a sphere, in contrast to a V-shaped Mach cone when it is a needle.

We take into account the effect of electrostatic force, Epstein drag force (\mathbf{F}_{EP}) and Polarization force (\mathbf{F}_p) in the momentum equation (Eq. 3) which are acting collectively on each particle. The Epstein drag force arises due to the collision between the background neutral gas molecules and dust particles, which can be expressed as,³¹,

$$\begin{aligned} \mathbf{F}_{EP} &= -\gamma_{EP} m_d \mathbf{v}_d(\mathbf{r}, t) \\ &= -\delta_{EP} \frac{4\pi}{3} n_n m_n v_n a^2 \mathbf{v}_d(\mathbf{r}, t), \end{aligned} \quad (5)$$

where, n_n, v_n, m_n are gas density, thermal velocity and mass for neutral gas molecules, respectively. a is the dust particle radius. γ_{EP} and δ_{EP} are the Epstein drag coefficient and a constant which depends on the interaction between the dust particles and gas molecules.

As discussed in Sec. I, when the electrons and ions are considered to be Boltzmannian, the polarization force can be expressed as^{27,28},

$$\mathbf{F}_P = -\frac{Q^2}{8\pi\epsilon_0} \frac{\nabla \lambda_d}{\lambda_d^2} \quad (6)$$

In the above situation when plasma satisfies the quasineutrality condition and there is no temperature gradient in the plasma then $\nabla \lambda_d$ can be expressed as,

$$\nabla \lambda_d = \frac{1}{2k_B T_i} \left(1 - \frac{T_i}{T_e}\right) \lambda_d e E. \quad (7)$$

Where $E = -\nabla \phi(\mathbf{r}, t)$, denotes the electrostatic field. Using the expression of $\nabla \lambda_d$ from Eq. (7) in Eq. (6) we get,

$$\begin{aligned} \mathbf{F}_P &= Q \frac{1}{16\pi\epsilon_0} |Q| e \left(1 - \frac{T_i}{T_e}\right) \frac{\nabla \phi(\mathbf{r}, t)}{\lambda_d k_B T_i} \\ &= -Z_d e \Re \nabla \phi(\mathbf{r}, t). \end{aligned} \quad (8)$$

Where the coefficient, $\Re (= \frac{1}{16\pi\epsilon_0} |Q| e (1 - \frac{T_i}{T_e}) / \lambda_d k_B T_i)$ determines the strength of plasma-particle polarization interaction²⁴. For typical complex plasmas, $a = 1 \mu\text{m}$, $Q = 10^3 e$, $\lambda_d = 10^{-4} \text{m}$ and $T_i = 0.03 \text{eV}$, we have $\Re = 0.12$. For larger sized dust grains which can retain higher

values of Q the value of \mathfrak{R} becomes larger and approaches unity. However, for $\mathfrak{R} > 1$ the polarization force exceeds the electrostatic force and the net force acting on the particles is no longer a restoring force which results in a growing unstable perturbation.

Replacing the expression of \mathbf{F}_{EP} and \mathbf{F}_p in the momentum equation (Eq. 3) we obtain the modified momentum equation as,

$$\frac{\partial \mathbf{v}_d(\mathbf{r}, t)}{\partial t} + \mathbf{v}_d \nabla \cdot \mathbf{v}_d(\mathbf{r}, t) = \frac{Z_d e}{m_d} (1 - \mathfrak{R}) \nabla \phi(\mathbf{r}, t) - \gamma_{EP} \mathbf{v}_d(\mathbf{r}, t). \quad (9)$$

In the perturbed situation, assuming a first order approximation, the dynamical variables $n_d(\mathbf{r}, t)$, $\mathbf{v}_d(\mathbf{r}, t)$, $\phi(\mathbf{r}, t)$, $n_e(\mathbf{r}, t)$ and $n_i(\mathbf{r}, t)$ about the unperturbed states are given by,

$$\begin{aligned} n_d(\mathbf{r}, t) &= n_{d0} + n_{d1}(\mathbf{r}, t), \\ \mathbf{v}_d(\mathbf{r}, t) &= \mathbf{v}_{d1}(\mathbf{r}, t), \\ \phi(\mathbf{r}, t) &= \phi_1(\mathbf{r}, t), \\ n_e(\mathbf{r}, t) &= n_{e0} + n_{e0} \left(\frac{e}{k_B T_e} \right) \phi_1(\mathbf{r}, t), \\ n_i(\mathbf{r}, t) &= n_{i0} - n_{i0} \left(\frac{e}{k_B T_i} \right) \phi_1(\mathbf{r}, t). \end{aligned} \quad (10)$$

The equilibrium electron density n_{e0} and ion density n_{i0} are related to the equilibrium dust density n_{d0} and the dust charge number Z_d by the charge neutrality condition,

$$n_{i0} = n_{e0} + n_{d0} Z_d. \quad (11)$$

Using equations (10) and (11) in equations (2), (4) and (9) we obtain,

$$\frac{\partial n_{d1}(\mathbf{r}, t)}{\partial t} + n_{d0} \nabla \cdot \mathbf{v}_{d1}(\mathbf{r}, t) = 0, \quad (12)$$

$$\frac{\partial \mathbf{v}_{d1}(\mathbf{r}, t)}{\partial t} = \frac{Z_d e}{m_d} (1 - \mathfrak{R}) \nabla \phi_1(\mathbf{r}, t) - \gamma_{EP} \mathbf{v}_{d1}(\mathbf{r}, t), \quad (13)$$

$$\nabla^2 \phi_1(\mathbf{r}, t) = 4\pi e [Z_d n_{d1}(\mathbf{r}, t) - Z_t \delta(\mathbf{r} - \mathbf{u}t)] + \lambda_d^{-2} \phi_1(\mathbf{r}, t). \quad (14)$$

Where $\lambda_d = \left[\frac{\epsilon_0 k_B}{e^2} \left(\frac{T_e T_i}{T_i n_{e0} + T_e n_{i0}} \right) \right]^{1/2}$, is known as dusty plasma Debye length as discussed before.

By using a partial Fourier transform with respect to \mathbf{r} and t dependencies

$$A(\mathbf{r}, t) = \int \frac{d\mathbf{k} d\omega}{(2\pi)^4} A(\mathbf{k}, \omega) e^{i\mathbf{k} \cdot \mathbf{r} - i\omega t}, \quad (15)$$

we can obtain the following expressions:

$$\begin{aligned} n_{d1}(\mathbf{r}, t) &= \frac{\beta}{(2\pi)^4} \int d\mathbf{k} d\omega e^{i(\mathbf{k} \cdot \mathbf{r} - \omega t)} \\ &\quad \times \frac{[1 - \epsilon(k, \omega)] \delta(\omega - \mathbf{k} \cdot \mathbf{u})}{\epsilon(k, \omega)}, \end{aligned} \quad (16)$$

$$\begin{aligned} \mathbf{v}_{d1}(\mathbf{r}, t) &= \frac{\beta}{(2\pi)^4 n_{d0}} \int d\mathbf{k} d\omega e^{i(\mathbf{k} \cdot \mathbf{r} - \omega t)} \\ &\quad \times \frac{\omega}{k^2} \frac{[1 - \epsilon(k, \omega)] \delta(\omega - \mathbf{k} \cdot \mathbf{u})}{\epsilon(k, \omega)} \mathbf{k}, \end{aligned} \quad (17)$$

where dielectric function $\epsilon(k, \omega)$ can be obtained by

$$\epsilon(k, \omega) = 1 - \frac{\omega_{pd}^2 (1 - \mathfrak{R})}{\omega(\omega + i\gamma_{EP})} \left(\frac{k^2 \lambda_d^2}{k^2 \lambda_d^2 + 1} \right) \quad (18)$$

with the dust plasma frequency $\omega_{pd} = \left(\frac{n_{d0} Z_d^2 e^2}{\epsilon_0 m_d} \right)^{1/2}$ and the ratio of charges $\beta = Z_t / Z_d$. It is clear from the above equations (Eqs. 16 and 17), both the perturbed density and the velocity are stationary fields in the frame of reference of the projectile particle moving with velocity \mathbf{u} .

The dispersion relation of low frequency dust acoustic wave can be obtained from Eq. (18) by setting $\epsilon(k, \omega) = 0$ ³². The modified dispersion relation in the presence of polarization force and Epstein drag force can be written as,

$$k^2 = k_d^2 \frac{\omega(\omega + i\gamma_{EP})}{\omega_{pd}^2 (1 - \mathfrak{R}) - \omega(\omega + i\gamma_{EP})}. \quad (19)$$

Where we have used $k_d = \lambda_d^{-1}$. From this modified

TABLE I. Dusty plasma parameters used for the numerical computations.

Test particle charge number (Z_t):	10000
Average charge on each particle (Q):	4007e
Dust particle radius (a):	4.5 (μm)
Inter-particle distance (d):	~ 230 (μm)
Equilibrium ion density (n_{i0}):	10^{14} (m^{-3})
Ion(electron) Temperature ($T_i(T_e)$):	0.1(3) (eV)

dispersion relation (Eq. 19), we can easily re-construct the dispersion relation of Piper and Goree³³ by setting $\mathfrak{R} = 0$ (absence of polarization force) and the dispersion relation of Khrapak *et al.*²⁴ when $\gamma_{EP} = 0$ (absence of Epstein drag force).

To study the propagation characteristic of Mach cone in detail, we solve the perturbed dust density n_{d1} from Eq. (16) and the perturbed velocity field vector \mathbf{v}_{d1} from Eq. (17) numerically. In accordance with the recent experiments³⁴, we choose our basic dusty plasma parameters, which are tabulated in Table-1. The other parameters such as, 2D dust density (n_{d0}), mass of MF particle (m_d), plasma Debye radius (λ_d) and dust frequency (ω_{pd}) are estimated with the help of these dusty plasma parameters. It is clear from the above equations (Eqs. 16 and 17), that the projectile particle velocity (\mathbf{u}) plays an important role to determine the wake structure formation which can be expressed in terms of Mach number, $M = u/C_s$ ($C_s = \lambda_d \omega_{pd}$ is being the dust acoustic velocity when the particle exerts only the electrostatic force). It is also clear from the above dispersion relation (Eq. 19), that the dust acoustic velocity changes with the change of polarization force coefficient (\mathfrak{R}). It indicates that the modified Mach number does not remain constant with the change of \mathfrak{R} . It is also worth mentioning that

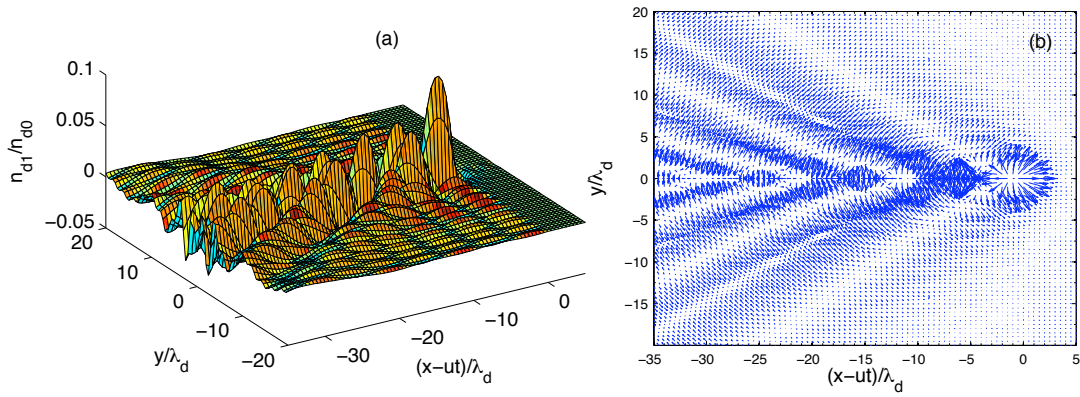


FIG. 1. (Color online). An example of Mach cone structures in presence of polarization force. a) Surface plot of perturbed dust density and b) dust velocity vector map for $M = 1.1$, $\gamma_0 = 0.01$ and $\Re = 0.4$.

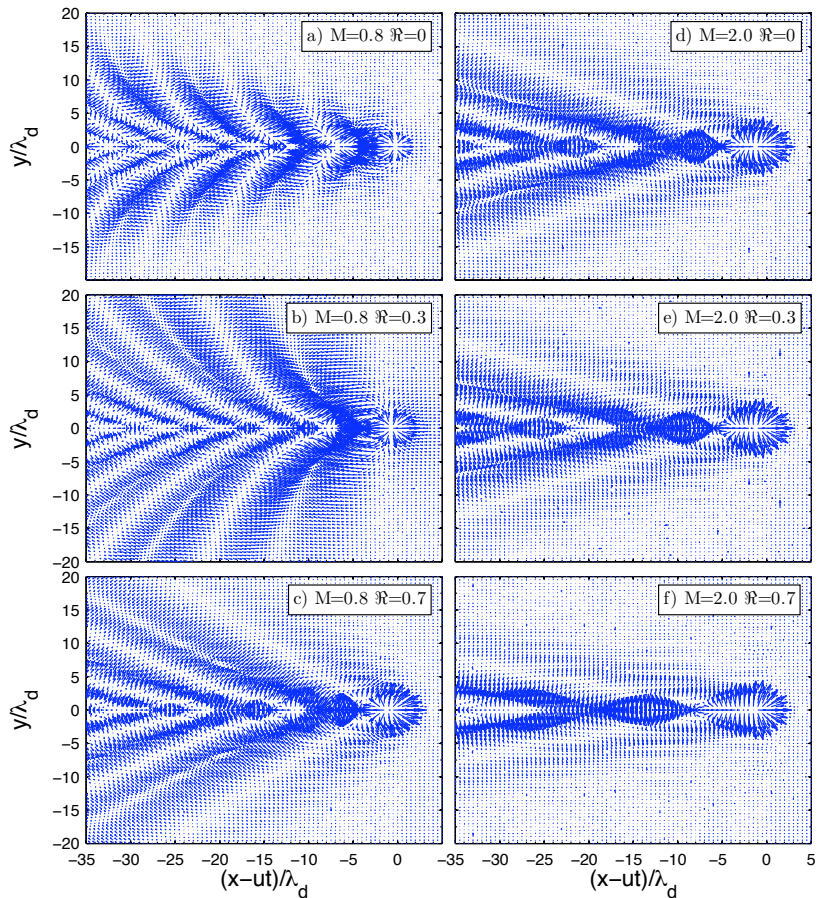


FIG. 2. (Color online). Map of the particle velocity vector (\mathbf{v}_{d1}) in case of weak damping $\gamma_0 = 0.01$ for a) & d) $\Re = 0$, b) & e) $\Re = 0.3$ and c) & f) $\Re = 0.7$. The left panel (a-c) is for $M = 0.8$ whereas the right panel (d-f) depicts for $M = 2.0$.

the normalized damping coefficient, $\gamma_0 = \gamma_{EP}/\omega_{pd}$, representing the background neutral gas pressure, is also an important factor to determine the Mach cone structures. Although in some cases, we assume that the Mach number (M) is a constant quantity, but in reality the Mach number changes with the change of \Re and γ_0 .

III. RESULTS AND DISCUSSIONS

Fig. 1(a) and (b) illustrate the typical normalized perturbed density (n_{d1}/n_{d0}) and velocity vector map of a lateral wake structure for a given Mach number ($M = 1.1$), Epstein drag coefficient ($\gamma_0 = 0.01$) and polarization force coefficient ($\Re = 0.4$). V-shaped Mach cone with

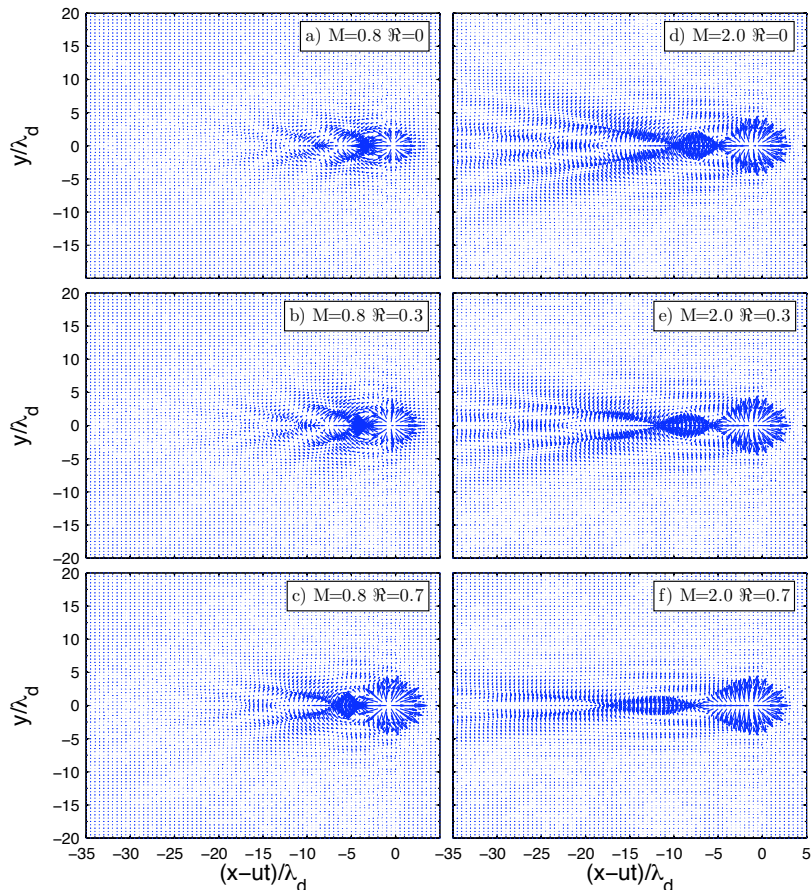


FIG. 3. (Color online). Map of the particle velocity vector (\mathbf{v}_{d1}) in case of strong damping $\gamma_0 = 0.2$ for a) & d) $\mathfrak{R} = 0$, b) & e) $\mathfrak{R} = 0.3$ and c) & f) $\mathfrak{R} = 0.7$. The left panel (a–c) is for $M = 0.8$ whereas the right panel (d–f) depicts for $M = 2.0$.

multiple wake structures can be clearly seen in both these figures. These patterns are caused by constructive and destructive interference of waves excited by the projectile particle, and their structures are determined by the wave dispersion properties of the medium as well as the disturbance-medium interaction. It also can be seen from the velocity field map (see Fig. 1(b)) that the structures consist of multiple cones, with the outermost being the most prominent. According to the earlier investigations of Mach cone in complex plasmas⁷, these multiple structures arise due to strongly dispersive nature of the dust acoustic waves. This figure also indicates that the direction of the dust particle motion is perpendicular to the cone wings and parallel to the direction of wave propagation. It confirms that the Mach cones are composed of compressional waves.

To study qualitatively the Mach cone structure for different values of projectile particle velocity in terms of Mach number and the polarization force, we first consider the case when the influence of damping is weak ($\gamma_0 = 0.01$). The left panel (a–c) of Fig. 2 shows the velocity field map of Mach cone for a constant value of Mach number ($M = 0.8$) at different values of polarization force coefficients, a) $\mathfrak{R} = 0$ (absence of polarization

effect), b) $\mathfrak{R} = 0.3$ and c) $\mathfrak{R} = 0.7$. The right panel (d–f) of Fig. 2 corresponds the same for $M = 2.0$ with the same values of \mathfrak{R} . It is clear from the left panel of the figure (Fig. 2(a–c)), that there is a prominent change in the structural properties of the Mach cone when \mathfrak{R} increases at a constant value of M and γ_0 . The number of multiple wake structures reduces while the opening angle decreases with the increase of \mathfrak{R} . The changes of opening angle with \mathfrak{R} at constant M can be explained from the dispersion relation (Eq. 19). With the increase of \mathfrak{R} the velocity of the DAWs decreases resulting in an increase of the modified Mach number. From the Mach-cone-angle relation, the opening angle reduces with the increase of this modified Mach number. It is also noticed that the curved nature of the wings of Mach cones becomes less significant as \mathfrak{R} increases. The bending structures of Mach cones were also predicted by Zhdanov *et al.*¹⁴. In their theoretical studies, they showed that either the time history of changes in the medium or the density gradient in the medium (or both) plays an important role to produce curved wings Mach cone structures. Although it is not clear in the present situation which factor is responsible to form the curved wings but the changes of the strength of polarization force certainly change the

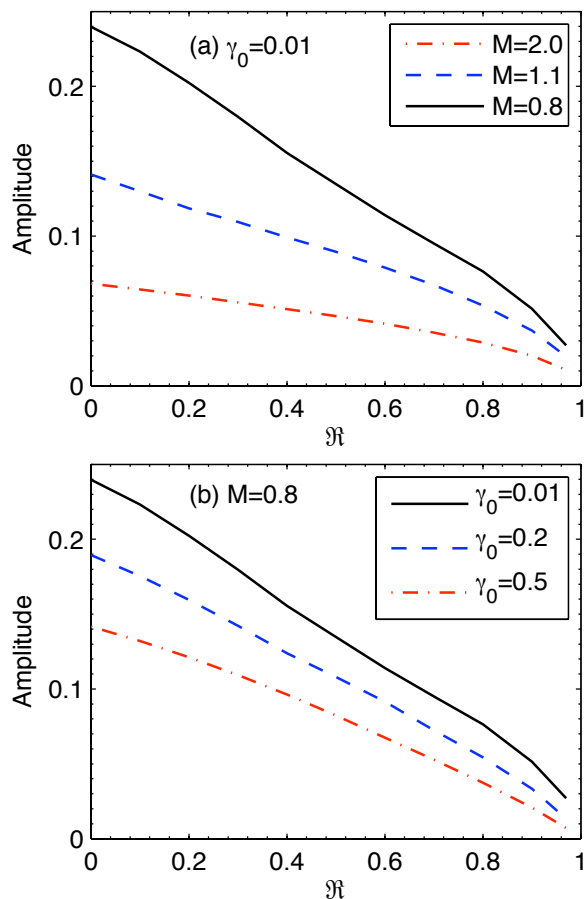


FIG. 4. (a) and (b) Variation of amplitude of normalized perturbed density with \Re for different values of (a) M at constant γ_0 and (b) γ_0 at constant M . In (a) solid, dashed, and dashed-dotted lines represent $M = 0.8, 1.1,$ and $2.0,$ respectively, at $\gamma_0 = 0.01$. Whereas in (b) solid, dashed, and dashed-dotted lines represent $\gamma_0 = 0.01, 0.2,$ and $0.5,$ respectively, at $M=0.8$.

inhomogeneity of the background plasma medium. It is also to be noted from the right panel of Fig. 2 that the opening angle and number of multiple structures reduces (even to one) due to the increase of Mach number. In case of higher Mach number ($M=2$), the curved nature of the wings in the Mach cone of velocity map also disappears.

In order to investigate the effect of dust-neutral collision frequency, we increase γ_0 from 0.01 to 0.2 and plot the velocity vector map in Fig. 3 keeping all other parameters constant. In accordance with earlier observations^{11,16,18}, the wakes are strongly damped and the oscillations in the wake region are smoothed out due to the decrease of the damping length, $l_d = Cs/\gamma_{EP}$. It is also seen from the above figure that the effect of higher dust-neutral collisionality reduces the number of multiple-wakes structures down to two or even one, irrespective of the Mach number and the strength of polarization force.

Fig. 4 depicts the variation of maximum amplitudes of perturbed dust density in 2D plasma crystal for a set of

Mach number and dust-neutral collision rate. Figure 4(a) represents the same when the dust neutral collision rate remains unchanged at $\gamma_0 = 0.01$ and the Mach number changes from 0.8 to 2. It is clear from this figure that the amplitude decreases with the increase of \Re for a given Mach number. It suggests that the increase of \Re influences the wake-field oscillations to be damped which shows a similar effect when γ_0 increases. As we have discussed earlier (see in Eq. 18) dielectric function $\epsilon(\omega, k)$ increases with the increase of \Re for a given dispersive medium with constant λ_d and ω_{pd} . It can be concluded from the expression of n_{d1} (Eq. 16) that the perturbed density decreases with the increase of strength of polarization force. For a given value of \Re , it should also be noted that the amplitude decreases with the increase of Mach number. Variation of maximum amplitude as a function of \Re shows similar trend when we change the dust-neutral collision damping rate from 0.01 to 0.5 at a constant value of Mach number ($M=0.8$) as shown in Fig. 4(b). This figure also suggests that the amplitude of density perturbation decreases with the increase of γ_0 for a constant \Re .

IV. CONCLUSION

We have studied theoretically the modifications arising in the Mach cone structure due to the presence of polarization force acting on the dust grains in an inhomogeneous plasma. Numerical results for the perturbed density and velocity vector in the dust layers exhibit Mach cone with the characteristic oscillatory wake patterns which is also observed in laboratory experiments^{15–21}. In our analysis, special attention is paid to the dependencies on the Mach cone structure for a wide range of polarization force at a given Mach number and the dust-neutral damping rate. Quantitatively, we have noticed that the amplitude of the perturbed dust density decreases with the increase of the polarization force coefficient. An experimental observation is needed to verify the polarization-induced change in the Mach cone structures.

- ¹H. Ikezi, Phys. Fluids **29**, 1764 (1986).
- ²H. Thomas, G. E. Morfill, V. Demmel, J. Goree, B. Feuerbacher, and D. Mohlmann, Phys. Rev. Lett. **73**, 652 (1994).
- ³Y. Hayashi, and K. Tachibana, Jpn. J. Appl. Phys. **33**, L804 (1994).
- ⁴J. H. Chu, and I. Lin, Phys. Rev. Lett. **72**, 4009 (1994).
- ⁵O. Havnes, T. Aslaksen, T. W. Hartquist, F. Li, F. Melandsø, G. E. Morfill, and T. Nitter, J. Geophys. Res. **100**, 1731 (1995).
- ⁶O. Havnes, F. Li, F. Melandsø, T. Aslaksen, T. W. Hartquist, G. E. Morfill, T. Nitter, and V. Tsyтович, J. Vac. Sci. Technol. A **14** 525 (1996).
- ⁷D. Dubin, Phys. Plasmas **7**, 3895 (2000).
- ⁸Z. W. Ma, and A. Bhattacharjee, Phys. Plasmas **9**, 3349 (2002).
- ⁹S. Zhdanov, S. Nunomura, D. Samsonov, and G. E. Morfill, Phys. Rev. E **68**, 035401(R) (2003).
- ¹⁰A. A. Mamun, P. K. Shukla, and G. E. Morfill, Phys. Rev. Lett. **92**, 095005 (2004).
- ¹¹L. J. Hou, Y. N. Wang, and Z. L. Mišković, Phys. Rev. E **70**, 056406 (2004).

- ¹²K. Jiang, L. J. Hou, Y. N. Wang, and Z. L. Mišković, *Phys. Rev. E* **73**, 016404 (2006).
- ¹³L. J. Hou, Z. L. Mišković, K. Jiang, and Y. N. Wang, *Phys. Rev. Lett.* **96**, 255005 (2006).
- ¹⁴S. Zhdanov, G. E. Morfill, D. Samsonov, M. Zuzic, and O. Havnes, *Phys. Rev. E* **69**, 026407 (2007).
- ¹⁵D. Samsonov, J. Goree, Z. W. Ma, A. Bhattacharjee, H. M. Thomas, and G. E. Morfill, *Phys. Rev. Lett.* **83**, 3649 (1999).
- ¹⁶D. Samsonov, J. Goree, H. M. Thomas, and G. E. Morfill, *Phys. Rev. E* **61**, 5557 (2000).
- ¹⁷A. Melzer, S. Nunomura, D. Samsonov, Z. W. Ma, and J. Goree, *Phys. Rev. E* **62**, 4162 (2000).
- ¹⁸V. Nosenko, J. Goree, Z. W. Ma and A. Piel, *Phys. Rev. Lett.* **88**, 135001 (2002).
- ¹⁹V. Nosenko, J. Goree, Z. W. Ma, D. Dubin, and A. Piel, *Phys. Rev. E* **68** 056409 (2003).
- ²⁰K. Jiang, V. Nosenko, Y. F. Li, M. Schwabe, U. Konopka, A. V. Ivlev, V. E. Fortov, V. I. Molotkov, A. M. Lipaev, O. F. Petrov, M. V. Turin, H. M. Thomas, and G. E. Morfill, *Eur. Phys. Lett.* **85**, 45002 (2009).
- ²¹M. Schwabe, K. Jiang, S. Zhdanov, T. Hagl, P. Huber, A. V. Ivlev, A. M. Lipaev, V. I. Molotkov, V. N. Naumkin, K. R. Sütterlin, H. M. Thomas, V. E. Fortov, G. E. Morfill, A. Skvortsov, and S. Volkov, *Eur. Phys. Lett.* **96**, 55001 (2011).
- ²²G. E. Morfill, H. M. Thomas, U. Konopka, H. Rothermel, M. Zuzic, A. Ivlev, and J. Goree, *Phys. Rev. Lett.* **83**, 1598 (1999).
- ²³A. Bose, and M. S. Janaki, *Phys. Plasmas* **13**, 012104 (2006).
- ²⁴S. A. Khrapak, A. V. Ivlev, V. V. Yaroshenko, and G. E. Morfill, *Phys. Rev. Lett.* **102**, 245004 (2009).
- ²⁵P. Bandyopadhyay, U. Konopka, S. A. Khrapak, G. E. Morfill, and A. Sen, *New J. Phys.* **12**, 073002 (2010).
- ²⁶A. A. Mamun and K. S. Ashrafi, and P. K. Shukla, *Phys. Rev. E*, **82**, 026405 (2010).
- ²⁷S. Hamaguchi, and R.T. Farouki, *Phys. Rev. E* **49**, 4430 (1994)
- ²⁸S Hamaguchi, and R. T. Farouki, *Phys. Plasmas* **1**, 2110 (1994).
- ²⁹I. H. Hutchinson, *Plasma Phys. Control. Fusion* **47**, 71, (2005).
- ³⁰P. Ludwig, W. J. Miloch, H. Kahlert, and M. Bonitz, *New J. Phys.* **14**, 053016, (2012).
- ³¹P. Epstein, *Phys. Rev.* **23**, 710 (1924).
- ³²M. Rosenberg, and G. Kalman, *Phys. Rev. E* **56**, 7166 (1997).
- ³³J. B. Pieper, and J. Goree, *Phys Rev. Lett.* **77**, 3137 (1996).
- ³⁴H. M. Thomas, G. E. Morfill, V. E. Fortov, A. V. Ivlev, V. I. Molotkov, A. M. Lipaev, T. Hagl, H. Rothermel, S. A. Khrapak, R. K. Suetterlin, M. Rubin-Zuzic, O. F. Petrov, V. I. Tokarev, and S. K. Krikalev, *New J. Phys.* **10**, 033036 (2008).